AMD4/AIS6-1
Invited

Monolithic Integration of Sn-Doped IGZO Transistor and Ferroelectric Memory for High-Density Memory Applications

Masaharu Kobayashi[1], Jixuan Wu[2], Fei Mo[2], Takuya Saraya[2], Toshiro Hiramoto[2], Kohei Nishiyama[3], Mototaka Ochi[3], Hiroshi Goto[4]

Masa-kobayashi@nano.iis.u-tokyo.ac.jp
[1]d.lab, School of Engineering, The University of Tokyo, 153-8505, Japan
[2]Institute of Industrial Science, The University of Tokyo
[3]Kobe Steel, Ltd., [4]Kobelco Research Institute, Inc.
Keywords: monolithic integration, IGZO, ferroelectric, memory

ABSTRACT

We have developed and integrated a mobility-enhanced FET and a wakeup-free ferroelectric capacitor by using Sn-doped InGaZnO (IGZTO), and demonstrated 1T1C memory cell operation for 3D embedded memory. An ultrathin IGZTO FET shows 2x higher mobility than IGZO FET. IGZTO also enhances ferroelectricity in HfO_2-based material. We have studied the impact of thin-film access transistor on 1T1C cell operation and investigated the physics of mobility enhancement by ab-initio calculations. IGZTO is a promising reliable and high-performance material for integrated device applications.

1 Introduction

The need of the proximity of high-density memory to processor core has been increasing for the last level cache in the conventional architecture and for machine-learning accelerators in AI chips. There are several choices of embedded memories such as eDRAM [1], MRAM [2] and PCRAM [3]. Those memory cells typically consist of a memory element and an access transistor which is usually a Si MOSFET. Then, an extra area is needed in a chip to place such access transistor in the FEOL layer. Moreover, the interconnect between the processor and the memory will cause overhead of energy and delay. If the access transistor can be made in BEOL layers, the RAM can be built directly on the processor and the interconnect overhead and the area penalty can be solved (Fig. 1).

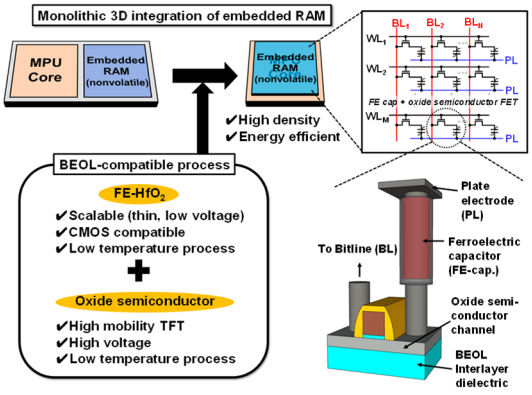

Fig.1 The proposed concept of monolithic 3D integration of oxide semiconductor FET and FE-HfO_2 capacitor for 1T1C embedded RAM application such as eDRAM and FeRAM.

Recently, oxide semiconductor such as InGaZnO (IGZO) [4-6] has been attracting attentions for integrated circuit applications because transistors can be placed in BEOL layers thanks to its low temperature process. Previously, we reported 1T1R cell operation of IGZO transistor and RRAM cell [7], where we emphasized the importance of mobility enhancement and high reliability of oxide semiconductor FET. As a memory element, ferroelectric (FE)-HfO_2 has been attracting attentions for its CMOS compatibility and scalability [8-11]. Therefore, the integration of oxide semiconductor FETs and FE-HfO_2 capacitors can be a feasible approach for 3D embedded RAM application such as eDRAM and FeRAM (Fig. 1).

In this work, we introduce Sn-doped IGZO (IGZTO), develop and integrate FETs and FE-capacitors (FE-caps), and demonstrate 1T1C operation. We discuss the characteristics of the integrated devices and the impact of IGZTO FET on 1T1C cell performance.

2 Design space of 1T1C cell

It is a critical question if the oxide semiconductor TFT can drive the FE-cap sufficiently fast for embedded RAM applications. We consider the design space of a 1T1C cell using an oxide semiconductor FET and a FE-cap. Fig. 2(a) shows the contour plot of switching time (t_{sw}) of FE cap calculated by FET current (I_{FET}) [12] and polarization charge. Polarization switching peak current

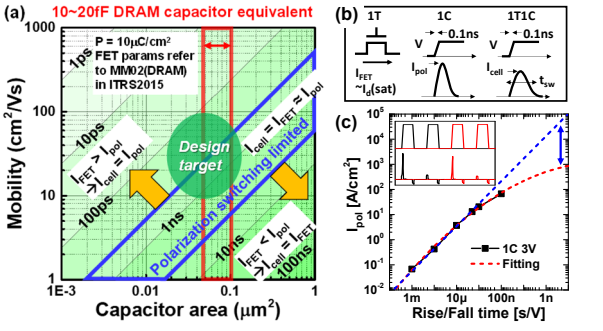

Fig. 2 (a) Contour plot of switching time (t_{SW}) of 1T1C cell calculated by FET current (I_{FET}) and polarization charge [12]. (b) Definition of I_{FET}, I_{pol}, and I_{cell}. (c) I_{pol} with different rise/fall times of voltage pulse.

(I_{pol}) is finite and can also limit t_{sw}. Fig. 2(c) estimates I_{pol} by extrapolating the measured peak current with different pulse rise/fall time. The extracted current sets the boundary in Fig. 2(a). The boundary determines which of I_{FET} or I_{pol} is the 1T1C cell peak current (I_{cell}). We found a design space where 10~100cm^2/Vs mobility oxide semiconductor FET can switch FE-cap in 1~10ns, which is applicable to embedded memory applications.

3 Device structure and Fabrication

We introduced Sn-doped IGZO (IGZTO) for FET in this work. This material has been developed for FPD purpose by co-authors [13]. Fig. 3 shows the PBTI characteristics of IGZO and IGZTO FETs made by the baseline process. IGZTO shows significant PBTI improvement. Fig. 4(a), (b), and (c) show the fabrication flow, the schematic of the device structure of a 1T1C cell, and the microscope image, for the proof-of-concept, respectively. An IGZTO FET was fabricated with a bottom-gate and a HfO_2 gate insulator with an ultrathin 8nm IGZTO layer. IGZTO was deposited by RF-sputter. A FE-cap was formed in the stack of TiN/$HfZrO_2$(HZO)/IGZTO/TiN. The HZO layer was deposited by ALD. Fig. 5 shows TEM images of an IGZTO FET and a FE-cap. Each layer was uniformly formed. With IGZTO cap, HZO layer was crystallized after RTA.

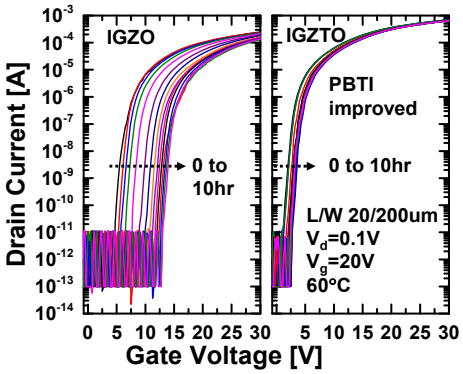

Fig. 3 Measured PBTI characteristics of IGZO and IGZTO FETs made by the baseline process. IGZTO FET shows significant improvement of PBTI reliability.

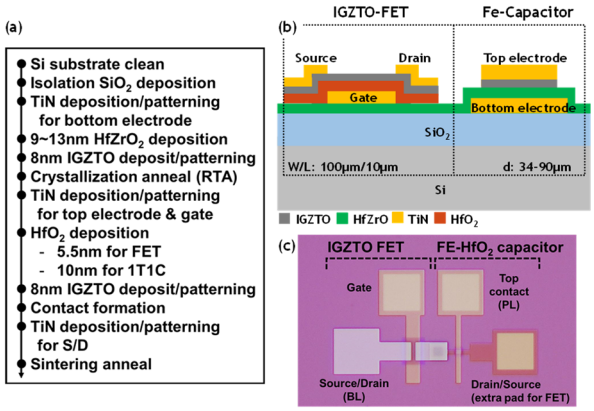

Fig. 4 (a) Fabrication process flow. An IGZTO FET was formed by bottom-gate structure with an ultrathin 8nm IGZTO. A FE-capacitor was formed in the stack of TiN/HZO/IGZTO/TiN. (b) Schematic of the device structure. (c) Microscope image. The IGZTO FET and the FE-cap are integrated into the same device.

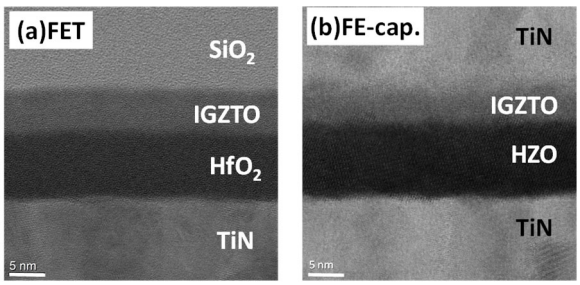

Fig. 5 Cross-sectional STEM images of (a) IGZTO FET and (b) FE-capacitor. Each layer was uniformly formed. With IGZTO capping, the HZO layer was crystallized after RTA.

4 Results and Discussions

4.1 FET and FE-cap characteristics

We characterized the fabricated IGZTO FET and compared to the reference IGZO FET. Fig. 6(a) and (b) show the I_d-V_g curves of the IGZO FET and the IGZTO FET, respectively. Normally-off operation, extremely low-leakage, nearly ideal subthreshold slope, and high drive current were obtained. Fig. 6(c) shows the I_d-V_d curves which show the 2× higher drive current in the IGZTO FET than in the IGZO FET. We extracted the effective mobility for both IGZO FET and IGZTO FET in Fig. 6(d). The IGZTO FET can achieve >20 cm^2/V·s with the ultrathin channel, which is also 2× higher than the IGZO FET. This mobility is consistent with our Hall mobility measurement, which indicates the advantage of oxide semiconductor FET without mobility degradation by high-k gate dielectric.

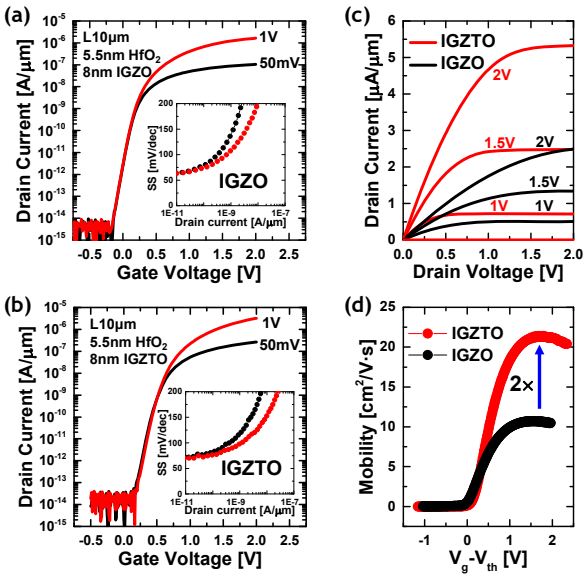

Fig. 6 (a) Measured I_d-V_g curves of the IGZO FET. The inset shows SS vs I_d. This is the reference device from Ref. [11]. (b) Measured I_d-V_g curves of the IGZTO FET. The inset shows SS vs I_d. Sharp cut-off characteristics are obtained. (c) Measured I_d-V_d curves of the IGZTO FET and the IGZO FET. IGZTO shows 2× higher I_{on}. (d) Measured effective mobility. IGZTO shows 2× higher mobility than IGZO.

To investigate the origin of high mobility in IGZTO FET, we extracted the temperature dependence of mobility in Fig. 7(a). The temperature dependence is smaller in the IGZTO FET, which indicates that the average potential barrier height is smaller in IGZTO FET based on the percolation transport theory [14] as shown in Fig. 7(b). The potential barrier height is attributed to the band edge fluctuation in an amorphous structure. To support this discussion, we used ab-initio calculations. Amorphous structure was formed by melt-and-quench method by molecular dynamic simulation. Then, the pseudo band-structure of random 10 samples of amorphous IGZO without and with Sn-substitute are calculated in Fig. 8. Small band edge fluctuation was obtained in IGZTO, which supports the discussion of the mobility enhancement.

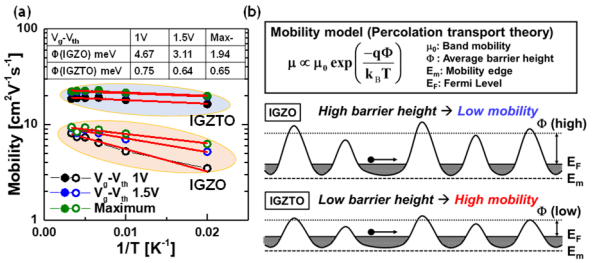

Fig. 7 (a) Temperature dependence of mobility and the extracted average barrier height at different biases. (b) Mobility model based on percolation theory [23]. IGZTO has a lower potential barrier height, which leads to higher mobility.

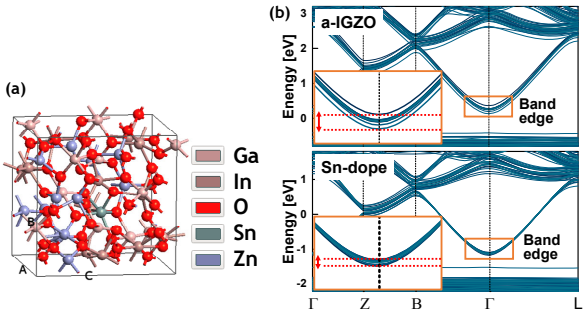

Fig. 8 (a) Atomic structure of an amorphous IGZO. (b) Calculated pseudo-band structures of a-IGZO and IGZTO. 10 samples are shown for each.

Next, we characterized the fabricated FE-caps with IGZTO capping. Fig. 9 shows the P-V curves of the FE-caps fabricated by 500℃ and 400℃ RTA. The 500℃ FE-cap has large P_r~20μC/cm^2. The 400℃ FE-cap also shows P_r~10μC/cm^2 with sharp switching, which is very promising for BEOL process compatibility by low temperature process. We also characterized the reliability of the FE-caps. Fig. 10 shows the endurance characteristics. Typically, FE-HfO_2 caps show "wake-up" behavior which is an unstable behavior in the initial cycles. The FE-cap in this work does not show wakeup behavior, which is attributed to the defect-less oxide-oxide interface between the HZO layer and the IGZTO layer. This result is consistent with our previous work with IGZO [15].

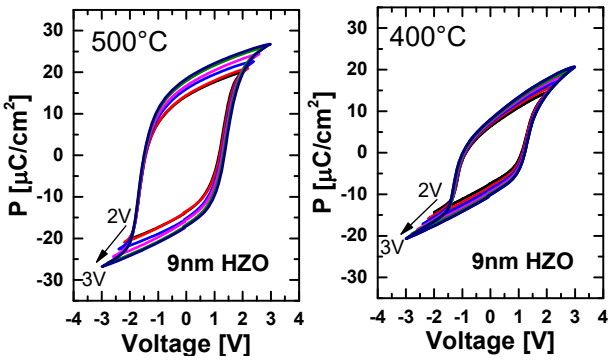

Fig. 9 (Left) Measured P-V curve of an IGZTO-capped HZO FE-capacitor with 500℃ RTA. (Right) Measured P-V curve of an IGZTO-capped HZO FE-capacitor with 400℃ RTA.

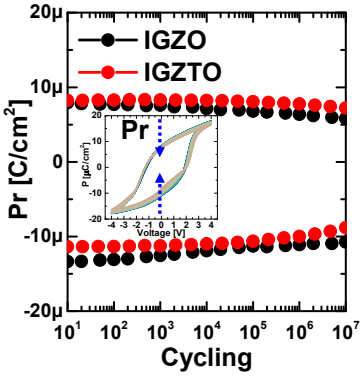

Fig. 10 Measured endurance characteristics without "wake-up" behavior (unstable characteristics in the initial cycles).

4.2 1T1C operation

We demonstrate write/read operation of a 1T1C cell by using the measurement scheme in Fig.11(a). 1T1C cell current (I_{cell}) is extracted by subtracting non-switching current from switching current.

Firstly, V_g dependence of the switching current behavior is shown in Fig. 11(b). Write operation can be slower than read operation due to the source-follower mode of the FET. I_{cell} is limited by I_{FET} and gets closer to I_{pol} as V_g increases. The increase of V_g is effectively equal to the increase of mobility, which corresponds to moving to the upper direction in Fig. 2(a) and indicates the importance of further mobility enhancement for faster cell operation. Read operation can be fast, especially if bitline-ground sensing scheme is used [16]. I_{cell} reaches I_{pol} as V_g increases.

Secondly, FE-cap size dependence is shown in Fig. 11(c). As the FE-cap size decreases, t_{sw} becomes shorter. The decrease of FE-cap size corresponds to moving to the left direction in Fig. 2(a). I_{cell} reaches I_{pol} for the smaller FE-cap in read operation.

Lastly, to estimate the performance in a scaled device size, we simulated a cell operation of a 1T1C cell with 0.1μm^2 FE-cap and scaled FET by SPICE simulation. The SPICE parameters were extracted from an IGZTO FET and a FE-cap in this work. The result shows ns operation and low energy consumption of ~100fJ/bit.

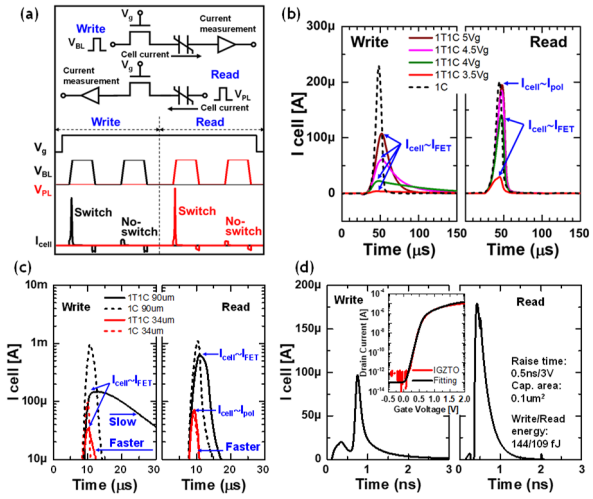

Fig. 11 (a) Measurement setup and typical measured waveform of a 1T1C cell. (b) The measured waveform of the 1T1C cell current with different V_g and 1C devices. (c) Measured waveform of the 1T1C cell current with different FE-capacitor sizes and 1C device. (d) SPICE simulation with 0.1µm^2 capacitor shows ns operation of 1T1C cell. The inset shows FET calibration.

5 Summary

We developed and integrated a mobility-enhanced FET and a ferroelectric capacitor by introducing Sn-doped IGZO (IGZTO), and successfully demonstrated 1T1C memory cell operation for 3D embedded memory. IGZTO FET shows 2x higher mobility than IGZO FET. IGZTO also enhances ferroelectricity and mitigates wake-up issue in HfO_2-based material. The physical origin of the high mobility can be the reduction of potential fluctuation by Sn atoms. IGZTO is a promising reliable and high-performance material for integrated device applications.

Acknowledgement

The authors like to thank Dr. Toshifumi Irisawa (AIST) for technical support. This work was partly supported by JST CREST (16815651), JSPS KAKENHI Grant Number JP18H01489.

References

[1] C-H. Lin, et al., IEDM, 74-76 (2014),
[2] S. H. Han, et al., IEDM, 215-218 (2020),
[3] F. Arnaud, et al., IEDM, 501-504 (2020),
[4] K. Nomura, et al., Nature, 432, 488 (2004),
[5] M. Oota, et al., IEDM, 50 (2019),
[6] C. C. Chang, et al., APL, 112, 172101 (2018),
[7] J. Wu, et al., VLSI Symp., 1-2 (2020),
[8] S. C. Chang, et al., IEDM, 605-608 (2020),
[9] J. Okuno, et al., VLSI Symp. 2020,
[10] L., Grenouillet, et al., VLSI Symp. 2020,
[11] Y.D. Lin, et al., IEDM, 346-349 (2019),
[12] ITRS2015,
[13] Ochi, M., et al., Proceedings of IDW, 308-311, 2018.
[14] S. Lee, et al., Applied Physics Letters 98.20 (2011): 203508,
[15] F. Mo, et al., Appl. Phys. Express, 13, 074005 (2020),
[16] S. Kawashima, et al., Journal of Solid-State Circuits 37.5 (2002): 592-598.